Published in final edited form as:
Adv Mater Technol. 2019 November ; 4(11): . doi:10.1002/admt.201900548.

Functionally Graded Knitted Actuators with NiTi-Based Shape Memory Alloys for Topographically Self-Fitting Wearables

Rachael Granberry,
Department of Design, Housing, and Apparel University of Minnesota

Kevin Eschen,
Department of Mechanical Engineering University of Minnesota

Brad Holschuh,
Department of Design, Housing, and Apparel University of Minnesota

Julianna Abel
Department of Mechanical Engineering University of Minnesota

Abstract

Advances in actuating fabrics can enable a paradigm shift in the field of smart wearables by dynamically fitting themselves to the unique topography of the human body. Applications including soft wearable robotics, continuous health monitoring, and body-mounted haptic feedback systems are dependent upon simultaneous body proximity and garment stiffness for functionality. Passive fabrics and fitting mechanisms are unable to conform around surface concavities and require either high elasticity or a multiplicity of closure devices to achieve garment fit. The design, manufacture, and validation of the first circumferentially contractile and topographic self-fitting garments composed of NiTi-based shape memory alloy (SMA) knitted actuators that dynamically conform to the unique shape and size of the wearer's body in response to a change of the garment's temperature is introduced. Advanced materials and systems innovations 1) enable novel garment manufacturing and application strategies, 2) facilitate topographical fitting (spatial actuation) through garment architectural design, and 3) provide tunable NiTi-based SMA actuation temperatures to enable actuation on the surface of human skin. This research represents a paradigm shift for wearable applications by redefining garment fit to fully topographical conformation to the wearer through advanced materials and structures design.

Keywords

functional fabrics; knitted actuators; NiTi; shape memory alloys

bth@umn.edu.

Conflict of Interest
The authors declare no conflict of interest.

Supporting Information
Supporting Information is available from the Wiley Online Library or from the author.

1. Introduction

Wearables, spanning consumer clothing to smart body-mounted devices, are plagued with fit and sizing challenges due to vast population anthropometric variability.[1,2] Accurate fit around a range of body shapes and sizes is a necessity for functional wearables, specifically those with integrated sensors and actuators that require stiffness of sufficient magnitude to enable structural anchoring at precise anatomical locations.[3] While polyether-polyurea copolymer (elastane) fabrics are capable of accomplishing accurate fit through undersized garment design, highly compliant garments fail to anchor functional components to the body. To achieve garment-body proximity and appropriate stiffness, designers compose sizing systems (S, M, and L) and mount hardware to less compliant materials that are fitted to the body with adjustable closures (e.g., laces, Velcro).[4,5] Despite the combination of fitting approaches, wearable device functionality remains highly variable due to garment fit inconsistencies between users, a limitation that ultimately inhibits usability.[6]

Multifunctional fabrics integrate advanced materials such as NiTi-based shape memory alloys (SMA), shape memory polymers (SMP), or carbon-nanotubes (CNT) and present a novel approach to the fit and sizing challenges of smart wearables that eliminate the bulk, complexity, and 1D nature of current approaches. Actuating multifunctional fabrics provide spatially and functionally distributed, tunable mechanical behavior that enables self-fitting and -stiffening around the variable topography of the human body. Prior work on actuating fabric structures has focused on traditional actuators (e.g., pneumatics, hydraulics, and motor-driven bowden cables) attached to or layered with passive fabrics.[7] Other research has attached 1D multifunctional actuator geometries (e.g., wire, springs) to traditional textile structures[8-10] These approaches are bulky, complex, and exhibit limited surface deformation. Prior work on spatially (3D) actuating multifunctional fabrics found that sophisticated shape-changing soft-robotic tasks such as translatory motion (length variability), rotational motion (rolling) and their superposition (wrinkle release), as well as significant volume changes can be accomplished.[11-16]

The most promising active material system for actuating fabrics is NiTi-based SMA, which offers a unique combination of high energy density, and large actuation displacements and forces. SMAs are advanced engineering materials that exhibit path-dependent thermo-mechanically induced martensitic phase transformations that enable the unique superelastic and shape memory effects. The phase transformations are introduced as a function of the applied materials stress, strain, and temperature, and depend on the thermo-mechanical loading history of the material.[17] The reversible transformation between the cubic austenite and the monoclinic martensite lattices enables variable stiffness, as well as the ability to undergo and recover large deformations of up to 8% (Figure 1a).[17] This specific self-fitting application leverages the shape memory effect of NiTi-based SMAs. Sufficient mechanical straining and stressing of the NiTi-based SMA wire results in a detwinning of the initially twinned monoclinic martensite at temperatures below the martensite finish temperature ($T < M_f$). Upon heating above the material-specific austenite finish temperature ($T > A_f$) the martensitic transformation to the cubic austenite lattices occurs and the imposed strains and stresses are recovered. The initial state of the wire is recovered through subsequent cooling

($T < M_f$), which forces the reverse phase transformation to the original unstructured twinned martensite lattice.

The phase transformation temperatures of NiTi-based SMA are highly programmable and can be tailored for a given application according to chemical composition and metallurgical heat treatment. Spanning martensite start (M_s) temperatures between −100 and 400 °C while preserving the shape memory effect, NiTi-based SMA renders the potential for a wide array of applications.[18,19] For binary NiTi alloys, manipulation of the Ni-volume fraction results in drastic variation of the transformation temperatures (A_f, A_s, M_s, and M_f) and thermal hysteresis. Slight Ni-richness ($c_{Ni} \approx 51.5$ at%) produces ≈200 °C lower transformation temperatures compared to marginally Ti-rich ($c_{Ni} \approx 49\%$) NiTi-based SMAs.[18] The partial replacement of Ni or Ti with ternary alloying agents modifies the transformation temperatures as a function of the concentration and number of valence electrons.[19] Heat treatment, specifically aging under defined times and thermo-mechanical loads, can cause the formation of precipitates (e.g., Ni_4Ti_3) and a consequential increase of the phase transformation temperatures through a decrease of the Ni-content in the matrix.[20]

Contractile SMA knitted actuators are actuating multifunctional fabrics composed of a single filament of SMA deformed and constrained into a traditional weft knit structure that can accomplish tunable actuation contractions between 4–50%.[21] As shown in Figure 1b, weft knits are composed of interlocking networks of geometrically identical loops organized in wales (columns) and courses (rows) forming knit patterns. Actuation contraction (ζ) is defined by the relation between the fully-martensitic knit length (blue) ($T < M_f$) and the contracted partially-austenitic knit length (red) ($T > A_f$) at constant macroscopically applied mechanical loading (Figure 1c). Tunable %-actuation contraction of contractile SMA knitted actuators is a function of two geometric design parameters, the wire diameter (d) and the knit index (i_k).[21] The knit index is a linear predictor of actuation contraction and nondimensional geometric number defined as the fraction of the loop enclosed area and the squared wire diameter (Figure 1b).[21] While the maximum %-actuation contraction can reach up to 50% at the specific peak actuation-contraction loading, for self-fitting wearables, the actuation contraction occurs in a near-zero load state.[21] In compliance with ISO standards, the prototypes were designed with respect to the %-actuation contraction at F = 0.5 N, which represents the minimum load at which knitted textiles produce consistent performance.[22] Under such loads, %-actuation contractions within the range of 4–40% are attainable.[21] Figure 1d depicts a multiplicity of knitted courses laid flat (left) and connected circumferentially to form a sleeve that translates uniaxial into circumferential contraction for circumferential fitting.

This work presents the design and validation of functionally graded knitted actuators with NiTi-based SMAs for topographically self-fitting wearables, highlighting the flexibility, and universality of the design process for a variety of fitting and actuation applications. Prototypes designed for multiple body regions using varying NiTi alloy compositions and thermomechanical properties were designed for leg and wrist showing topographical and self-fitting. The garment for the leg, a large and geometrically complex region of the body was implemented using commercially available, high-temperature NiTi (Dynalloy, Flexinol, A_f = 90 °C) and validated for contractile ability and conformity to the leg topography using

3D marker tracking. Improved topographical conformity and body-temperature actuation are presented in a wrist sleeve manufactured from custom, small batch, Ni-rich NiTi material with novel transformation properties engineered by Fort Wayne Metals.

2. Results and Discussion

The thermo-mechanical behavior of SMA knitted actuators guides the operation for self-fitting wearable, detailed in Figure 1e. 1) In its initial state, the pre-donned martensite state (PDMS), the self-fitting garment begins oversized and compliant (Figure 1e-1). In this state, the SMA material is composed of twinned and detwinned martensite, determined by the strains and stresses imposed during the knit manufacturing process. The knitted loops allow for relative translatory and rotational displacements to enable structural compliance. 2) Subsequent to the PDMS, the garment is subject to don forces as it is pulled over the leg and reaches the deformed martensite state (DMS), Figure 1e-2. As the knitted actuator is strained macroscopically, both the twinned and detwinned martensite are elastically deformed and a partial transition from twinned to detwinned martensite occurs at the lattices that are subject to sufficiently high stresses. Translation and rotation of knitted loops also contribute to extension. 3) Post don, the external forces are released and the self-fitting garment relaxes from Figure 1e-2-3 into the donned relaxing martensite state (DRMS). The residual displacements between points 1 and 3 of Figure 1e are caused by material and knit architectural effects. Elastic deformations are recovered in both the twinned and detwinned martensite; however, no reverse transformation from detwinned to twinned martensite occurs. Additionally, frictional forces at the contact points of interlacing knitted loops resist full-recovery of the imposed donning displacements. 4) Self-fitting and self-stiffening are initiated by an increase in thermal load above the austenite finish temperature of the self-fitting garment. The garment recovers thermoelastic deformations and the garment circumference dimensions decrease as the garment enters into the fitting partially-austenitic state (FPAS). The SMA material transitions from twinned and detwinned martensite to detwinned martensite and austenite, a state that is referred to as partially-austenitic. The change of lattice structure from martensite to austenite causes both material stiffening as well as garment circumference reduction due to partial recovery of knitted loop bending deformations imposed in the manufacturing process. At point 4, the body and garment dimensions are equal, therefore, further phase transition from martensite to austenite does not provide additional displacements. 5) Because thermal loading continues to transition twinned and detwinned martensite to austenite, the knitted loops interlock into a higher friction configuration into the tight partially-austenitic state (TPAS). The reconfiguration (architectural stiffening) generates circumferential forces (Figure 1e-5) which are translated to the wearer's body as compressive pressures. The self-fitting garment is doffed while in a TPAS by applying external forces to stress the garment off the body. Similar to an elastic band, these doffing forces, which follow the partially-austenitic loading curve, are low as long as the garment is designed to exert compressive pressures below 10 mmHg. Garments designed to exert greater wearing forces for compressive pressure applications would require a zipper-release, or another quick-release mechanism, to enable doffing.

The design process for self-fitting wearables was grounded in anthropometric analysis and guided by performance (i.e., %-actuation contraction), comfort (i.e., pressure),

manufacturability, tactile acuity, weight, and cost requirements. Figure 2a depicts the methodology for defining garment actuation contraction performance using anthropometry and minimum garment dimensions based on donning logistics.[23] Uniaxial contraction is accomplished upon heating above the austenite finish temperature through the recovery of bending deformations and formation of ridges between alternating courses of knit and purl loops, which are mirrored opposites. The %-actuation contraction (ζ) of SMA knitted actuators is defined as

$$\xi = \frac{l_m - l_a}{l_m} \quad (1)$$

the normalized difference between the fabric's martensite length (l_m) and austenite length (l_a) at a given load and, while following the engineering strain definition, named in clear distinction to material strains.[21] The complex thermo-mechanical loading state of SMA knitted actuators with variable strains and stresses inhibits the assumption of full austenitic transformation at A_f, which is defined as a stress-free transformation temperature. The dimensions of a participant's leg collected for the initial prototype (Figure 2a-red) are plotted along with the minimum garment dimensions (Figure 2a-blue) to enable don/doff, specifically to pull the garment over the heel. Similarly, the design requirements for a wrist sleeve were determined by plotting the body dimensions along with the minimum garment dimensions to enable the sleeve to be pulled over the maximum hand circumference (further described in the Supporting Information). The %-actuation contraction requirements for self-fitting garments are thus defined by the percent difference between the garment dimensions and the body dimensions at each circumferential cross-section. Assuming the austenitic fabric length (l_a) equals the circumference of the body (c_b) when fitted ($l_a = c_b$) and the martensitic fabric length (l_m) equals the circumference of the garment (c_g) when oversized ($l_m = c_g$), analysis in Figure 2a reveals that self-fitting garments should have a functionally graded design to prevent over-constricting certain areas of the body (e.g., thigh) and under-fitting others (e.g., ankle). Comfort requirements were established to retain garment pressures below that of medical compression garments.[24] The critical force (F_{crit}) at which the critical pressure is reached (p_{crit} = 1300 Pa) was determined for the variable limb cross-sectional radius (r) per standard cross-sectional fabric width (w = 0.02 m), assuming rigid cylinders.[23,24] The 11 panels that make up the self-fitting leg sleeve are depicted in Figure 2b. The SMA knitted actuator performance was compared to body dimensions for the determination of the required number of courses to accomplish the desired actuation displacements (Figure 2c) with additional detail provided in the Supporting Information. Each panel was knit on a manual weft knitting machine (Taitexma TH-860) with pre-conditioned SMA wire (Dynalloy Flexinol, A_f = 90 °C). The final prototype is depicted in Figure 2d in a compliant, oversized martensitic state (left) and in a stiff, fitted austenitic state (right).

An innovative approach toward a quantitative measure of fit (traditionally a qualitative process) was developed through 3D, noncontact displacement and strain measurements from 3D marker tracking. The experimental validation methods were designed to measure the success of the self-fitting design by 1) assessing the fit quality through comparison of the

fitted garment dimensions in relation to the dimensions of the participant's leg geometry, and by 2) characterizing the accomplished %-actuation contractions in the fitting process.

The interpolated surfaces of the leg replica (gray), the fitted garment (red), and the oversized garment (blue) (Figure 3a) demonstrate successful self-fitting performance; however, suggest improvements could be made at the interface of the knee and lower thigh ($y = 39$ cm). To enable quantitative analysis of the nonplanar anatomy, a curved slice that follows the largest z-dimensions of the leg replica was extracted. As shown in Figure 3a center and right, while the mean dimensional difference between the leg replica and the fitted garment was 1.6 mm, the minimum garment thickness of 0.4 mm reduces the difference to 1.2 mm. The maximum dimensional difference between the leg replica and the fitted garment (5.2 mm) occurs at the transition from thigh to knee ($y = 39$ cm), an area of complex geometry that exhibits large concavities and convexities.).

In addition to garment-body proximity, 3D marker tracking data was used to evaluate garment actuation contraction and shows garment over-contraction in some areas of the body and under-contraction in others. Figure 3b displays the average %-actuation contractions (ζ_{avg}) derived from the normalized difference of Euclidean distances between neighboring markers aligned in the x-directions from the oversized and fitted garment analyses of both the anterior and lateral views. Measurements toward the ankle ($y = 5$–15 cm) depict average overperformance caused by a larger than predicted martensite garment dimension. In contrast, measurements at the knee ($y = 31$ cm) depict average undercontraction of up to 7% points. Figure 3b right splits the anterior and lateral views to show that, while the self-fitting marker measurements above the ankle ($y = 11$–46 cm) show under-contraction in the anterior view, over-contraction occurs in the lateral view. Only lower calf cross-sectional areas ($y = 10.2$ cm), which are approximately cylindrical, show identical %-actuation contraction in both lateral and anterior views, suggesting performance is dependent on the surface topography upon which contractile SMA knitted actuator fabrics actuate. The consistent under-contraction of the self-fitting garment around the knee, specifically at $y = 32$ cm where both lateral and anterior views under-contract, motivates further investigation of body surface conditions.

A self-fitting garment can contract fully and not be proximal to body concavities just as the garment can be proximal to the body and not fully contracted across body convexities; therefore, the quantitative analysis was supplemented with a topographical analysis to demonstrate the effect of noncylindrical body shape on purely contractile SMA knitted actuators. As depicted in Figure 3c, each cross-section was divided into medial, lateral, anterior, and posterior quadrants. The equivalent radial coordinate (r) of each cross-section was analyzed with respect to the angular coordinate (θ). Five spliced lateral and anterior radial coordinate plots chosen as extreme examples were then matched with the %-actuation contraction performance plots in Figure 3c. Comparing Figure 3b,c numbers 1–5, areas of topographical concavity or relatively mild convexity contracted adequately, while garment under-contraction occurred at angles of extreme topographical convexity. Here concavity and convexity are defined analogous to convex functions; If a line segment between any two $r(\theta_1)$ and $r(\theta_2)$ is consistently equal or greater than the values of $r(\theta)$ between θ_1 and θ_2, the topography is called concave. Extreme concavities are those concavities that maximize the

area enclosed by the line segment and $r(\theta)$. Topographical convexities follow the same definition for $-r(\theta)$.

To improve the fit of SMA knitted actuators, specifically to conform around body topography, we created modified grid patterns to achieve fully spatial actuation for one body cross-section between the knee and thigh ($y = 32$ cm, Figure 3b), chosen for its complex geometry. The cross-section was 3D printed and three variable grid pattern prototypes were manufactured. Figure 4a,b present the SMA knitted actuator panels in their actuated states both around the body cross-section a) and under uniaxial loading b). The first contractile SMA knitted actuator panel was fabricated according to the original self-fitting garment design at the region of the leg from which the cross-section was extracted ($d = 0.3$ mm, $\dot{\imath}_k = 72$ mm/mm) (Figure 4a-1 isometric, a-2 cross-section, and b-1 linear). Fit was evaluated through a novel contact sensing method that measured garment-cross-section contact at 28 discrete points. While the results of the 3D marker tracking show adequate fabric actuation contraction at concave body contours, the contact sensing investigation confirms that the fabric does not conform around concavities, but rather bridges the surface. Consequently, a second prototype sleeve (Figure 4a-2,b-2) was designed with purl-only regions placed at concave areas of the body to force the fabric to curve inward and knit-only regions placed at convex areas of the body to force the fabric to curve outward. Figure 4c, depicts the actuation behavior of the three knitted architectures: 1) garter, 2) purl-only, and 3) knit-only. While the prototype sleeve (Figure 4a-2,b-2) does accomplish nonplanar actuation and curls in directions appropriate for body topography, the junctures between the two knit patterns are discontinuous and the fabric lifts off the surface. Contact sensing of sleeve 2 shows diminished contact (54% < 70%) in relation to sleeve 1 due to abrupt changes in knit pattern. A third prototype sleeve (Figure 4a-3,b-3) includes transitions between architecture types to soften the curling actuation of nonplanar architectures. Figure 4a-3 depict increased fit (i.e., 86% contact), or proximity to the body, through gradient transitions between garter, purl-only, and knit-only knitted architectures.

The design and manufacturing procedures for a topographically fitting garment was applied to a self-fitting wrist sleeve designed to slide over the hand and conform to the anatomy of the wrist solely powered by the participant's body heat. The final prototype was designed with a small batch of custom, Ni-rich NiTi manufactured by Fort Wayne Metals and composed of 54.5–57.0% Ni with ternary elements O+N, C, Co, Cu, Cr, Fe, and Nb (0.010–0.050% maximum per additive). The material was cold-worked into a 0.142 mm diameter wire and straight-annealed. DSC testing (depicted in Figure 5a) was completed to ascertain thermal transition temperatures ($A_f = 36.5$ °C, $A_s = 23.5$ °C, $M_s = -50.5$ °C, and $M_f = -73.5$ °C). While the austenite finish temperature ($A_f = 36.5$ °C) is higher than mean skin temperature in thermally comfortable environments ($T_s \approx 35$ °C; $T_{amb} \approx 32$ °C), the thermal transition temperatures were low enough to demonstrate actuation on the human body with minimal applied heat. X-ray diffraction (XRD) informs about the microstructural composition of the Fort Wayne Metals material at $T = -85$ °C (martensite) and $T = 45$ °C (austenite) (Figure 5b). Stress–strain data was collected to demonstrate the material behavior at temperatures around the application use-case ($T =$ [25, 35, and 45 °C]) as well as below the martensite finish temperature ($T = -73$ °C) (straight wire, $d = 0.076$ mm, Figure 5c).

Figure 5c highlights the temperature-dependence of the material upper plateau stress. Cyclic stress-strain data for the material ($d = 0.127$ mm) is depicted in Figure 5d.

The first self-fitting, self-stiffening prototype made for direct contact with the human body is depicted in Figure 6. The prototype was designed to stretch over the subject's largest hand circumference (20 cm) and contract to achieve the dimensions of the subject's wrist (15 cm). To achieve the required actuation contraction ($\zeta_{req} = 25\%$), a large knit index ($\dot{\iota}_k = 124$ mm/mm, $d = 0.142$ mm) was selected to accomplish actuation contraction up to 36% (Figure 6a). Garter and knit-only patterns were used within the knitted architecture to mirror the topography of the wrist (Figure 6b). Specifically, a knit-only knit architecture was used around curved surfaces (i.e., proximal, medial surfaces, and over the ulna head). A garter knit architecture was used distal and proximal to the ulna head to conform around the cylindrical protrusion.

Consistent with garment operations outlined in Figures 1e and 6c depicts topographical self-fitting: 1) PDMS–The prototype is initially exposed to temperatures below the martensite finish temperature ($M_f = -73.5$ °C) and brought back to room temperature ($T = 20$ °C, $F = 0$ N), which is below the austenite start temperature ($A_s = 23.5$ °C) (Figure 6c-1). 2) DMS–The compliant, martensitic sleeve is pulled over the largest part of the hand ($T = 20$ °C, $F = 3.2$ N) (Figure 6c-2). 3) RMS–The prototype is positioned on the subject's wrist while remaining slightly oversized ($T = 20$ °C, $F = 0$ N) (Figure 6c-3). 4) FPAS–The prototype is warmed by body heat, both the adjacent skin and the palm of the other hand ($T = 45$ °C, $F > 0$ N) (Figure 6c-4). 5) TPAS–The stiff and fitted prototype conforms around the curvature of the wrist bones after warming ($T = 45$ °C, $F = 0.7$ N) and exerts forces well below those that would apply 10 mmHg of compression to the wrist ($F_{crit} = 1.9$ N) (Figure 6c-5). The forces required to doff the garment are represented by the thermomechanical response of the device while fully warmed ($T = 45$ °C). The doffing path in Figure 6c shows that the device can be pulled off the wrist at low forces ($F_{doff} = 4.7$ N), similar to an elastic band. While the thermal transition temperatures of the material require future adjustment (i.e., some austenite may be present at $T = 20$ °C), the prototype confirms the feasibility of a self-fitting, self-stiffening wearable designed for direct contact with the human body.

3. Conclusion

NiTi-based SMA knitted actuators present a paradigm shift for smart wearables, spanning consumer, medical, and aerospace spheres, by enabling no-power, topographically conforming garments through innovations in NiTi-based material systems and garment design processes. The presented work surpasses traditional apparel methodologies and will enable unpowered, automated fit through the exact setting of material transformation temperatures to accommodate a wide range of user dimensions. Design and manufacturing processes implemented with multiple prototypes highlight the flexibility and applicability of the approach to any body region and garment size. Multiple NiTi-based SMA materials with distinct thermomechanical properties are used to fabricate prototypes that demonstrate the adaptability of the material system. Because garment tightening and garment-body conformity are inequivalent, novel spatial actuation contraction is leveraged to achieve topographical conformity, a quality that is unachievable with passive fabrics or uniaxial

actuators. The resulting topographically self-fitting wrist sleeve demonstrates the functionality and feasibility of a NiTi-based SMA knitted actuators in the design of a new class of smart wearables.

4. Experimental Section

Materials:

NiTi-based 90 °C Flexinol actuator wire was purchased from Dynalloy, Inc. in 0.152, 0.203, 0.254, and 0.305 mm diameters and used without any material modifications. The custom NiTi-based actuator wire used in the self-fitting wrist sleeve was provided by Fort Wayne Metals in a 0.152 mm diameter only. The custom material was composed of 54.5–57.0% Ni and contained tertiary elements O+N, C, Co, Cu, Cr, Fe, and Nb (0.010–0.050% maximum per additive). The custom material was heat treated during the manufacturing process and was not modified after the material was received.

Calculation for Garment Dimensions:

To calculate the number of knitted courses and wales required to achieve the dimensions and shape of each of the 11 knit panels depicted in Figure 2b, fabric force-length data collected was scaled so that any given leg circumference was positioned between its paired fabric's austenite and martensite lengths at low load (50 g), as shown in Figures 1e and 2c.[21] The number of knit courses (fabric length) was decreased if the body circumference (c_b) was less than or equal to austenite fabric length (l_a) so that the garment does not have to use maximum %-actuation contraction potential to successfully self-fit (Figure 1e, $c_b < l_a$). Conversely, the number of knit courses was increased if the body circumference (c_b) exceeded the martensite fabric length (l_m) because in this scenario the unactuated garment would already fit (Figure 1e, $c_b > l_m$). Additionally, the number of knit courses was increased if the force at the body circumference (c_b) and austenite fabric length (l_a) intersection (Figure 1e-4) exceeded the critical force (F_{crit}). The number of wales was determined through traditional, passive knit scaling methodologies by counting the number of wales per predetermined dimensions (here 2 cm) and scaling per panel width specifications.

SMA Knit Actuator Thermomechanical Architectural Shakedown:

Once knit, each panel was thermally loaded between 20 and 120 °C under constant mechanical loading ($F = 0.5$ N) for 15 cycles to enable the material to settle into its new knitted configuration[25,26]

3D Marker Tracking Setup:

An experimental test stand replicating the shape and dimensions of the participant's leg was cast from Densite K-5 plaster for testing the active fitting garment, which was manufactured with 90 °C Flexinol wire. The garment was donned and doffed over the foot and external heat was applied with heat guns. Bow-tie markers were sewn to the garment in the anterior and lateral-views using a 4 × 20 marker pattern to capture the circumferential contraction of the garment along its length. Two CMOS cameras with frame rates of 20 f/s tracked the markers to produce a 3D point cloud for each frame during the fitting procedure.

3D Marker Tracking Procedure:

The garment was donned on the experimental test stand and thermo-mechanically loaded following the load path displayed in Figure 1e. The experimental procedure was repeated ten times for both the front and side views. Repeated measures and statistical analysis were required due to variable oversized reference configurations post donning in the martensite state. The oversized garment, similar to traditional clothing, can fall into a nearly infinite number of equilibrium states due to low architectural stiffness (e.g., wrinkle formation). Because the %-actuation contraction (ζ) is dependent on the initial garment dimensions, oversized garment variability affects the measured %-actuation contraction. Stereo digital imaging for 3D marker tracking has a limited field of view because both cameras are required to continuously capture every marker. Rather than capturing a cumulative 360° view of the garment, actuation contraction performance was sampled at the anterior and lateral leg views. Capturing 180° provided a representative sample of concave and convex topographies and contractile performances of SMA knitted actuator fabrics around the human body.

3D Marker Tracking Analysis:

The 3D marker tracking algorithm (Correlated Solutions VIC3D) outputs a Cartesian coordinate point cloud for each frame captured during the thermo-mechanical loading of the self-fitting garment. Despite the approximately circular leg geometry which would be most efficiently described with polar coordinates, this analysis was conducted in the Cartesian system to comply with the standard anatomical terms of directional description (x-axis = transverse axis, y-axis = vertical axis, z-axis = sagittal axis), depicted in Figure 3a. The Euclidean distance (E) was calculated between adjacent markers of each circumferential marker quadruplet (a, b, c, and d) and the %-actuation contraction (ζ) was determined in the oversized fully-martensitic and the fitted partially-austenitic garment. 3D surface plots were created from the point clouds of the leg replica, the fitted garment, and the oversized garment for the fit quality analysis. Delauney triangulation was used to interpolate between the discrete points and generate the continuous surface. Potential sources of measurement error stem from marker thickness, garment thickness, and the marker attachment method, as well as errors introduced in the marker tracking calibration, imaging process, and the interpolation process for the generation of the analyzed surfaces.

Contact Sensing Procedure:

A custom setup was designed to experimentally collect contact information between the 3D printed knee cross-section and the SMA knitted actuator sleeve prototypes (Figure 4a-1-3) to observe the influence of knitted architecture on garment fit (i.e., conformity) around body topography. Resistance measurements were used to identify contact. An electrode was permanently connected to the sleeve and electrically conductive materials (¼″ copper tape) were placed around the knee cross-section at 28 discrete locations (see Figure S9 in the Supporting Information). Upon contact, the measured resistance settles to values below 3 Ω whereas it is unpredictable but of significantly higher magnitude without established contact. A data acquisition device (NI-6341) enabled 8 simultaneous resistance measurements and four contact measurement runs were performed for each of the sleeve samples 1–3. The

resistance data was processed to identify the upper envelope signal (Hilbert transform) and avoid faulty contact information stemming from sign-changes in resistance while no contact was established (Figure S10, Supporting Information). The contact cut-off resistance (3 Ω) was defined as the maximum in-contact resistance measurement error to accurately identify the in-contact (>3 Ω)/no-contact (<3 Ω) signals. Additional details are provided in the Supporting Information. For each sleeve, the contact condition at measurement points 1–28 was identified as a "contact," "flutter," and "no contact" condition based on resistance data (Figure S11, Supporting Information). The value 1 was assigned for "contact," 0.5 for "flutter," and 0 for "no contact." Table S1 (Supporting Information) provides the evaluation for all sleeves and measurement points. 86% of contact measurements were identified to be in-contact for sleeve 3 compared to 70% for sleeve 1 and 54% for sleeve 2.

X-Ray Diffraction Procedure:

Microstructural characterization of the custom Fort Wayne Metals NiTi material was performed on a Bruker D8 Advance Cu-source, theta-theta diffractometer. The diffractometer enables the characterization of thermally-induced martensite and austenite states at respective material phase transition finish temperatures ($M_f = -73.5$ °C, $A_f = 36.5$ °C) through cooling/heating between −190 and 300 °C. The NiTi wire was cut into innumerable pieces and randomly distributed on the measurement stage to recreate conditions resembling powder to enable the measurement of all diffraction peaks despite the 1D detector limitation. This is a necessary step to avoid missing peaks that could only be resolved in higher dimension detectors because of the known presence of texture in the wire. Experiments were performed in a nitrogen environment to avoid the formation of crystals upon cooling. Figure 5b presents the 2θ-intensity plots of the austenitic state and the martensitic state with potential R-phase and precipitate peaks.

NiTi Tensile Characterization Setup:

Characterization of Fort Wayne Metals custom NiTi wire samples and the fabricated wrist sleeve were conducted on an Instron machine (model #3365) housed in a thermal chamber (calibration, −80 to 150 °C) and equipped with a 25 lb load cell (±1% of force reading from 0.6–0.2 N). Pneumatic side-action grips pressurized to 50 psi were used to grip straight wire samples. A mechanical couple (see Figure S12 in the Supporting Information) was used to hold the wrist sleeve in place during testing.

NiTi Thermal Response Characterization Procedure:

Multiple FWM NiTi samples from the same sample batch (0.076 mm diameter) were exposed to four different temperatures (i.e., 45, 35, 25, −73 °C) and mechanically strained to observe resulting material stresses. Each sample was strained at a rate of 4×10^{-4} 1/s and subsequently unloaded at each fixed temperature (Figure 5c).

NiTi Cyclic Characterization Procedure:

Cyclic stress–strain behavior was observed by repeated loading and unloading one FWM NiTi sample ($d = 0.127$ mm) at a temperature above the austenite finish temperature ($T = 70$ °C) at a rate of 8×10^{-5} 1/s (Figure 5d).

Wrist Band Tensile Characterization Procedure:

The experimental, self-fitting wrist band designed with custom FWM NiTi material was evaluated through force-displacement testing to validate the garment operation and forces throughout the donning process. The testing setup, detailed in Figure S12 in the Supporting Information, shows that the circular wrist band was tested at half scale (i.e., body circumference (c_b = 15 cm), equivalent length in testing setup ($l = c_b/2$ = 7.5 cm) and scaled up in Figure 6c. The wrist band was cooled below the martensite finish temperature (T = −73 °C) before beginning the test procedure. 1) The thermal chamber temperature was raised to room temperature (T = 20 °C). 2) Holding the temperature at room temperature (T = 20 °C), the circular sleeve was extended (0.01 mm s^{-1}) to a length that would enable donning over the circumference of the hand (l = 10 cm) and held for 5 min. 3) The garment was then mechanically unloaded (0.01 mm s^{-1}) and 4) returned to the length of the wrist (l = 7.5 cm), followed by another 5 min hold. Because the test was conducted through displacement-control, the recovery from a relaxed martensite length to the wrist circumference length was accomplished by the testing instrument rather than through garment actuation contraction. Here, actuation contraction is represented by the distance between the length at which martensite forces are no longer legible by the load cell (F = 0.2 N, l = 8.4 cm) and the length representing the wrist circumference (l = 7.5 cm). 5) The chamber was then heated above body skin temperature (T = 45 °C) and held for 15 min to observe an increase in blocked force (l = 7.5 cm). After the 15 min hold, the wrist sleeve displacement was increased again to observe the forces required to doff the garment while still warm (T = 45 °C). These experiments were carried out with the full, informed consent of the subjects, in accordance with all local laws and with the approval of all relevant ethics bodies. Due to the harmless nature of the work, body-worn prototypes were worn only by the authors, in accordance with the University of Minnesota's Institutional Review Board (IRB) which does not require review for self-experimentation with devices of Non-Significant Risk (NSR).

Supplementary Material

Refer to Web version on PubMed Central for supplementary material.

Acknowledgements

K.E. and R.G. contributed equally to this work. R.G., K.E., and J.A. developed the self-fitting garment operation. K.E. led the garment 3D marker tracking data collection and analysis procedures, developed the topographical investigation method, conducted XRD analysis of the custom NiTi material, and developed the setup used to gather and analyze contact sensing data. R.G. designed the anthropometric analysis procedure, developed the custom NiTi material requirements in collaboration with FWM, led the development of the knitted garment patterns, developed manufacturing procedures, and conducted thermomechanical performance analysis of the custom material. J.A. and B.H. guided the direction, motivation, and methods for the work. This work was supported in part by a NASA Space Technology Research Fellowship (Grant #80NSSC17K0158), Minnesota's Discovery, Research, and Innovation Economy Robotics, Sensors, and Advanced Manufacturing (MnDRIVE RSAM) Initiative, and the University of Minnesota Office of the Vice President for Research UMII MnDRIVE Graduate Assistantship. Thank you to Fort Wayne Metals for supplying the nickel-rich NiTi material. Thank you to the University of Minnesota Polymer Characterization Facility and Charles Weinberg from the University of Minnesota Design of Active Materials and Structures Lab for assisting with DSC testing. Thank you for support from the University of Minnesota's Wearable Technology Lab, specifically Heidi Woelfe, for coordinating time on the Instron machine.

References

[1]. Gill S, Text. Prog 2015, 47, 1.

[2]. Gordon CC, Churchill T, Clauser CE, Bradtmiller B, McConville JT, Anthropometric Survey of US Army Personnel: Methods and Summary Statistics, Anthropology Research Project Inc, Yellow Springs, OH, USA 2012.

[3]. Granberry RM, Duvall J, Dunne LE, Holschuh BT, in Proc. Int. Symp. Wear. Comp, ACM, New York, NY 2017, pp. 10–17.

[4]. Cappello L, Meyer JT, Galloway KC, Peisner JD, Granberry RM, Wagner DA, Engelhardt S, Paganoni S, Walsh CJ, J. Neuroeng. Rehabil 2018, 15, 1. [PubMed: 29298708]

[5]. Awad LN, Bae J, O'Donnell K, De Rossi SMM, Hendron K, Sloot LH, Kudzia P, Allen S, Holt KG, Ellis TD, Walsh CJ, Sci. Transl. Med 2017, 9, eaai9084. [PubMed: 28747517]

[6]. Panizzolo FA, Galiana I, Asbeck AT, Siviy C, Schmidt K, Holt KG, Walsh CJ, J. Neuroeng. Rehabil 2016, 13, 43. [PubMed: 27169361]

[7]. Cappello L, Galloway KC, Sanan S, Wagner DA, Granberry RM, Engelhardt S, Haufe FL, Peisner JD, Walsh CJ, Soft Rob. 2018, 5, 662.

[8]. Chenal TP, Case JC, Paik J, Kramer RK, in Proc. IEEE/RSJ Conf. Intell. Rob. Syst, IEEE, New York, NY 2014, pp. 2827–2831.

[9]. Yuen MC, Bilodeau RA, Kramer RK, IEEE Rob. Autom. Lett 2016, 1, 708.

[10]. Holschuh BT, Newman DJ, Aviat., Space Environ. Med 2016, 87, 2.

[11]. Abel J, Luntz J, Brei D. Smart Mater. Struct 2013, 22, 125001.

[12]. Han MW, Ahn SH, Adv. Mater 2017, 29, 1700244.

[13]. Harrington MJ, Razghandi K, Ditsch F, Guiducci L, Rueggeberg M, Dunlop JWC, Fratzl P, Neinhuis C, Burgert I, Nat. Commun 2011, 2, 1.

[14]. Foroughi J, Spinks GM, Aziz S, Mirabedini A, Jeiranikhameneh A, Wallace GG, Kozlov ME, Baughman RH, ACS Nano 2016, 10, 9129. [PubMed: 27607843]

[15]. Maziz A, Concas A, Khaldi A, Stålhand J, Persson NK, Jager EWH. Sci. Adv 2017, 3, e1600327. [PubMed: 28138542]

[16]. Kumar B, Hu J, Pan N, Biomaterials 2016, 75, 174 [PubMed: 26513411]

[17]. Schetky LM, Sci. Am 1979, 241, 74 [PubMed: 504982]

[18]. Frenzel J, George EP, Dlouhy A, Somsen C, Wagner MF, Eggeler G, Acta Mater. 2010, 58, 3444.

[19]. Zarinejad BM, Liu Y, Adv. Funct. Mater 2008, 18, 2789.

[20]. Khalil-Allafi J, Dlouhy A, Eggeler G, Acta Mater. 2002, 50, 17.

[21]. Eschen K, Abel J, Smart Mater. Struct 2019, 28, 025014.

[22]. Tensile properties of fabrics, ISO 13934-1, 2013.

[23]. Eschen K, Abel J, Granberry R, Holschuh B, in Proc. ASME Conf. Smart Mater. Adapt. Struct. Intell. Syst, ASME, New York, NY 2018, pp. 1–20.

[24]. Medical Compression Hosiery: Quality Assurance, RAL-GZ 387/1, 2008.

[25]. Churchill CB, Shaw JA, Proc. SPIE 2008, 6929, 69291F.

[26]. A Smirfitt J, J. Text. Inst., Trans 1965, 56, 6.

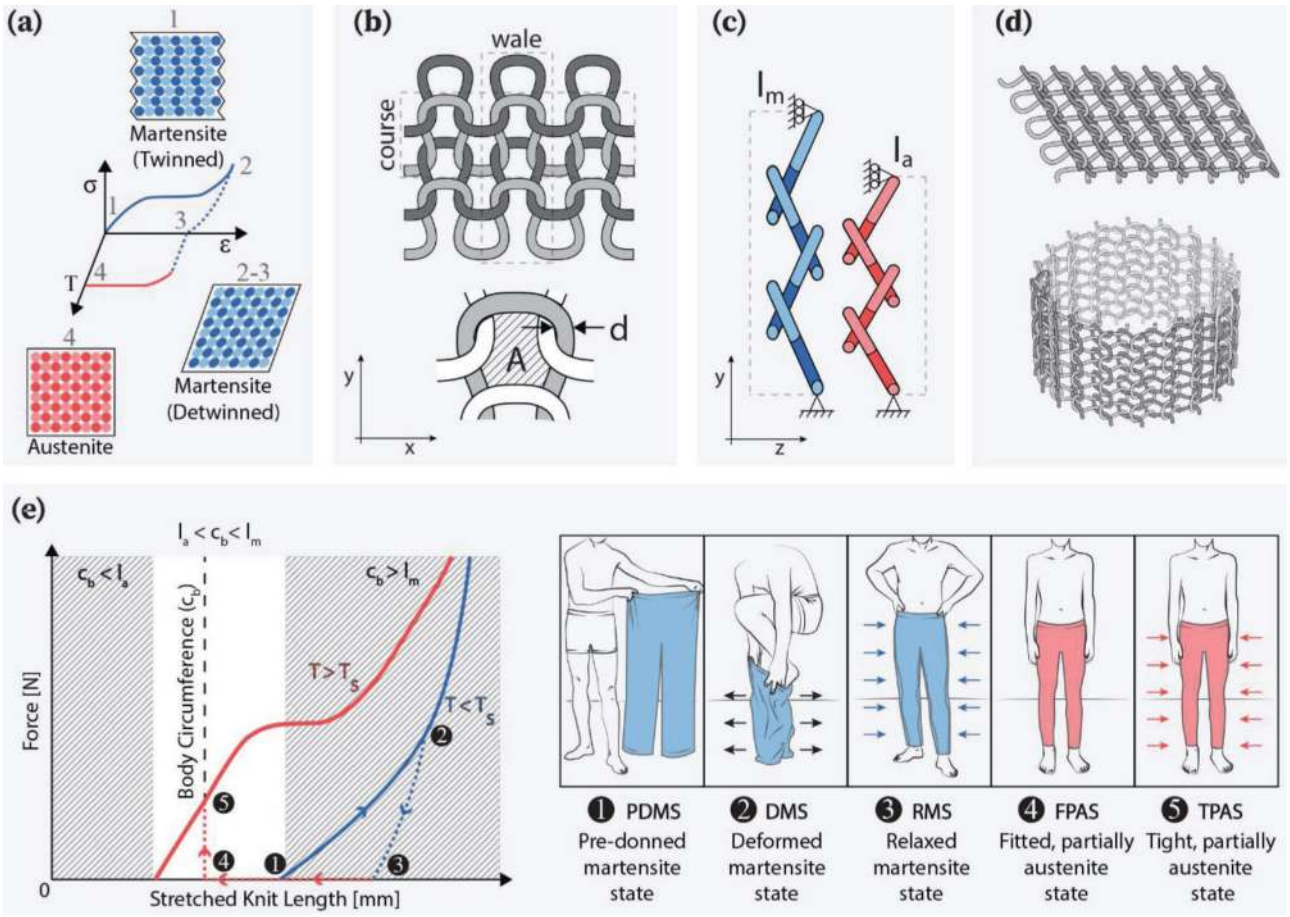

Figure 1.

a) Shape memory alloys are characterized by recoverable strain achieved through changes in material crystalline structure. Applied stresses turn twinned martensite 1) into detwinned martensite 2,3). Application of thermal loads recovers the mechanically imposed strains and stresses as the material returns to an austenite state 4). b) Knit geometry and geometric design parameters, including SMA wire diameter (*d*) and loop enclosed area (*A*). A column of knitted loops forms a wale and row of knitted loops form a course. c) Knit architectures (i.e., garter knit) can produce planar contractions between martensite (blue) and austenite (red) material phases, producing a distinct martensite length (l_m) and austenite length (l_a) per applied load. d) Knit fabrics are constructed through successively added courses. To achieve circumferential contraction, fabrics are wrapped with courses parallel and wales perpendicular to the length of the body. e) Self-fitting garments designed with knitted SMA experience the following stages through use; 1) Pre-donned martensite state (PDMS): The garment begins oversized, compliant, and fully martensitic. 2) Deformed martensite state (DMS): Outward forces are exerted that partially detwin the martensitic garment as it is pulled over the body. 3) Relaxed martensite state (RMS): Martensite relaxation occurs once the garment is on the body. 4) Fitted, partially austenite state (FPAS): The garment contracts when actuated to recover its austenite length, achieving the dimensions of the body and 5) tight, partially austenite state (TPAS): tightens around that form.

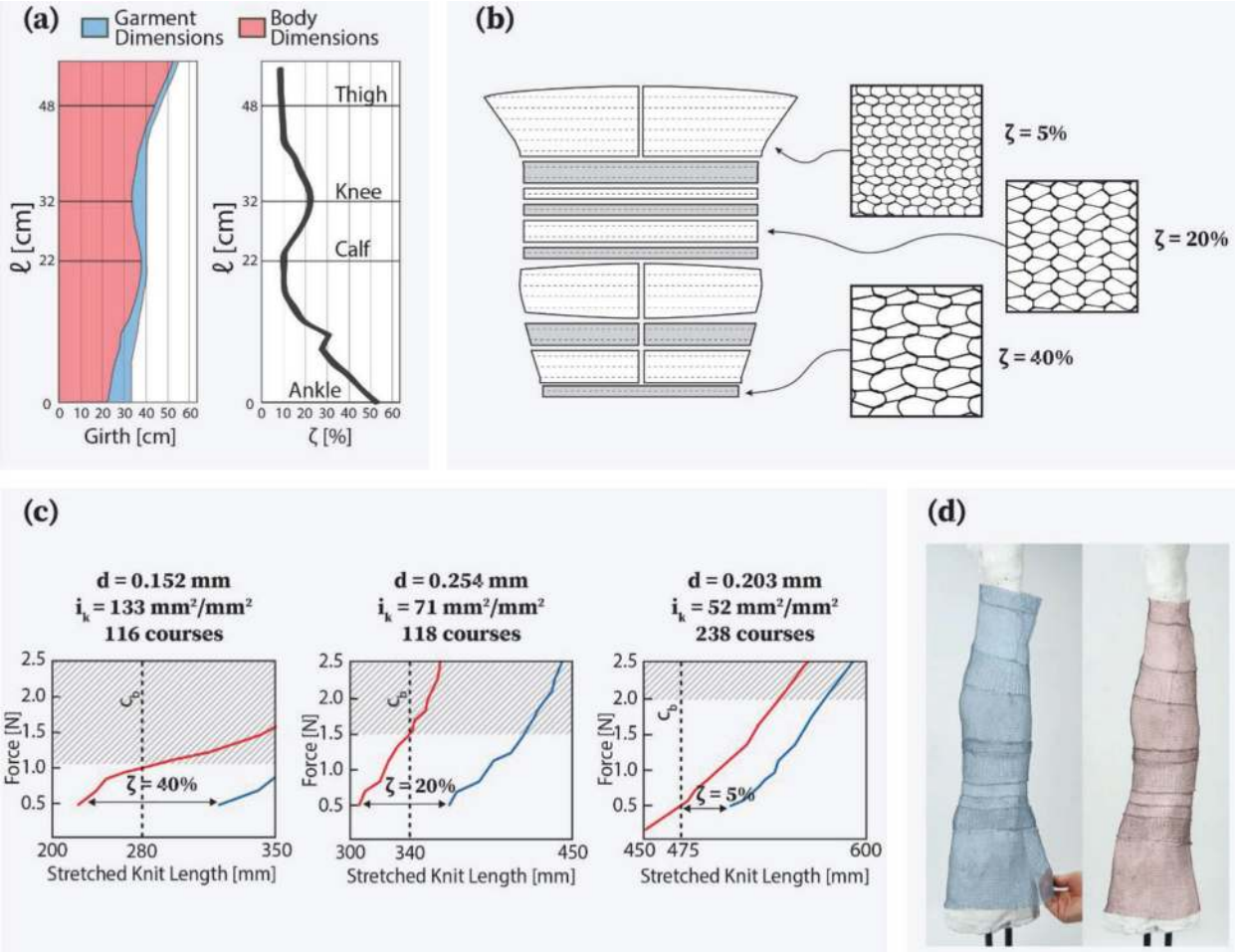

Figure 2.

a) Required self-fitting garment actuation contraction [%] determined through anthropometric analysis. Functionally graded garment performance is required to produce even pressures on the body. b) Garment pattern derived from anthropometric analysis. Ten segmented panels make up the garment, each with unique dimensions and actuation contraction performance mirroring the body. Panels with nonrectangular forms are split at center front so that all shaped edge conditions can be manufactured identically. c) Garment pattern dimensions were determined by pairing body circumference (c_b) measurements with the appropriate SMA knitted actuator force-displacement curves. Knitted courses were added or subtracted to position the body circumference (c_b) between the austenite knit length (l_a) and martensite knit length (l_m) to keep forces below 10 mmHg. d) The completed self-fitting garment is depicted in unactuated (left) and actuated (right) states.

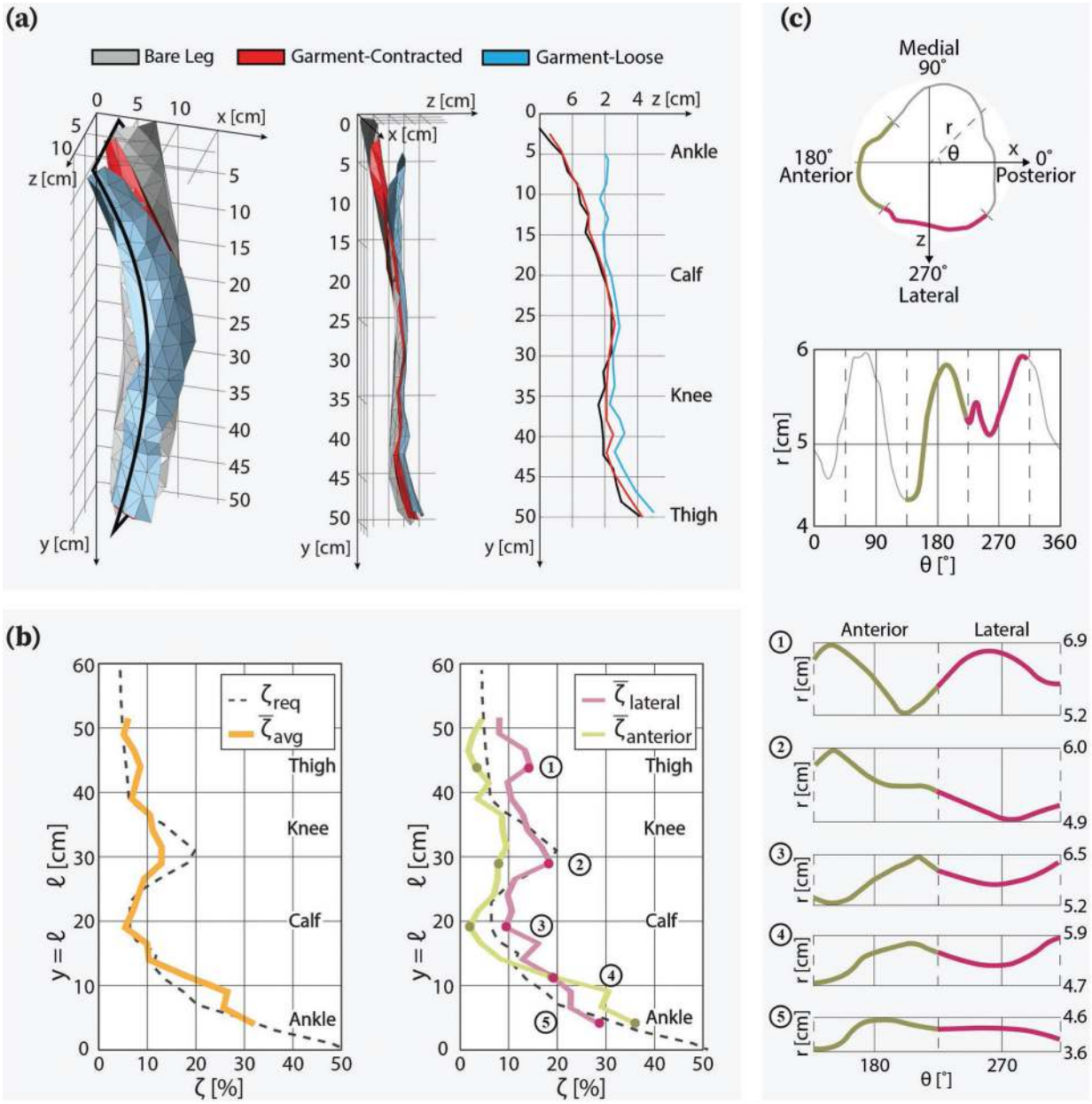

Figure 3.

a) The bare leg replica (gray), the unactuated garment surface (blue), and the actuated garment surface (red) were interpolated. A 2D slice was extracted to evaluate fit in terms of garment proximity to the body. b) (left) Measured actuation contraction was averaged from 10 anterior marker tracking trials and 10 lateral marker tracking trials (right). Anterior and lateral marker tracking trails were split to evaluate differences in performance based on area of the body. c) Cross-sections were gathered from the leg replica through 3D scanning. Deviation from perfectly cylindrical geometries was analyzed for each cross-section by plotting the radial coordinate against the angular coordinate. The anterior and lateral derived radial magnitudes were extracted and evaluated for their convexity or concavity. Plots 1–5

depict examples of regions with adequate actuation contraction as well as inadequate actuation contraction (anterior 1, 2, and 3), characterized by sharp, convex peaks.

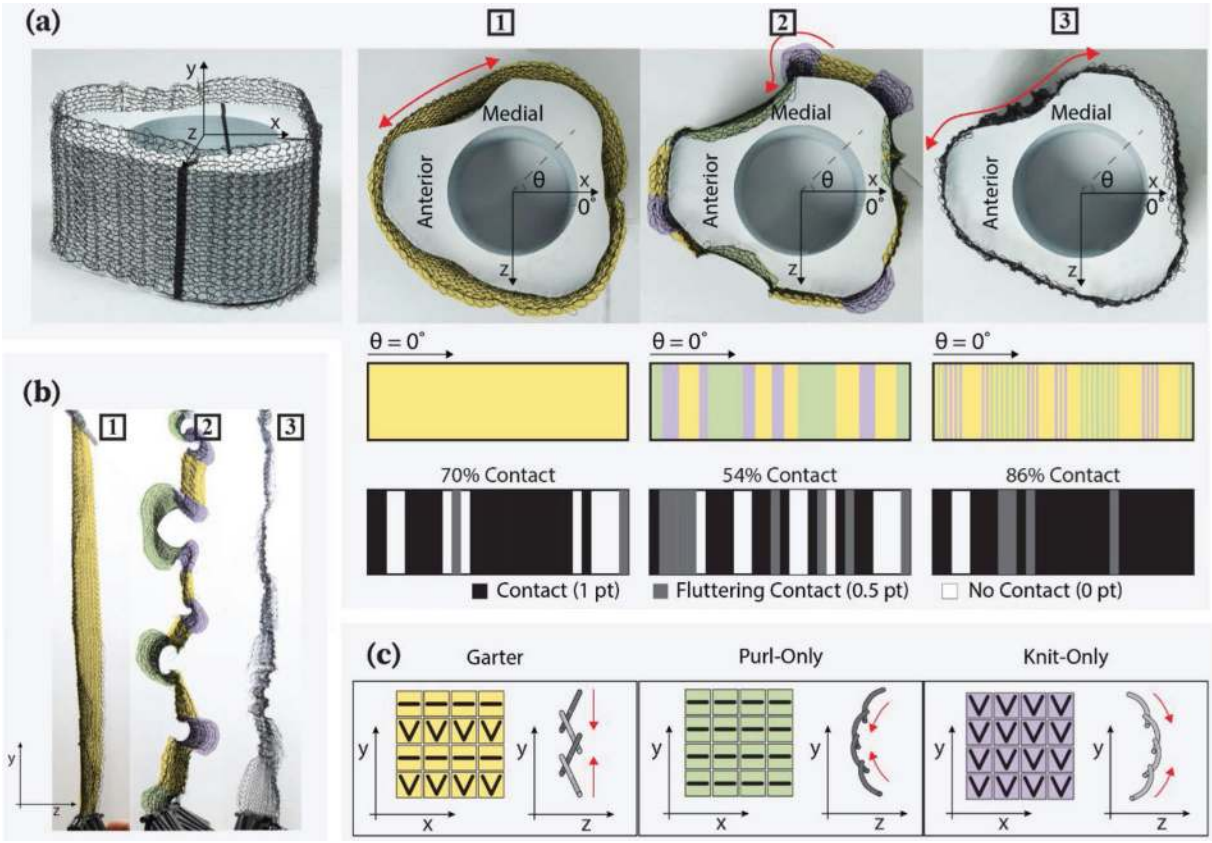

Figure 4.

a) A 3D printed leg cross-section was used to evaluate the fit of contractile SMA knitted actuators around complex body topography. Contact sensing at 28 discrete points around the circumference of the cross-section was used to evaluate fit (i.e., contact) between samples 1–3 of varying knitted architectures. 1) A garter knit panel replicating the geometry used in the self-fitting garment prototype shows bridging over concave surfaces and results in approximately 70% contact with sensing points. 2) A second panel constructed with modified knit geometries, specifically alternating garter, knit-only, and purl-only architectures, shows improved fit around concave and convex surfaces; however, the transitions between the three different architectures produce areas that lift off the surface, which resulted in poor contact performance of 54%. 3) A third panel constructed with blended garter, knit-only, and purl-only architectures produces improved fit around concave and convex surfaces with 86% contact with sensing points. b) Actuation contraction of panels a) 1–3 depicted under planar loading. 1) The garter knit panel remains planar upon actuation. 2) The alternating garter, knit-only, and purl-only panel take sharp, non-planar shape change. 3) The blended garter, knit-only, and purl-only panel produces gradated, non-planar shape change more appropriate for leg topography. c) Knit patterns are an organized grid of knitted loops combined in series and in parallel.[11] Garter knit patterns are formed by alternating knit courses and purl courses while purl-only and knit-only are formed by repeating stitches throughout the grid.

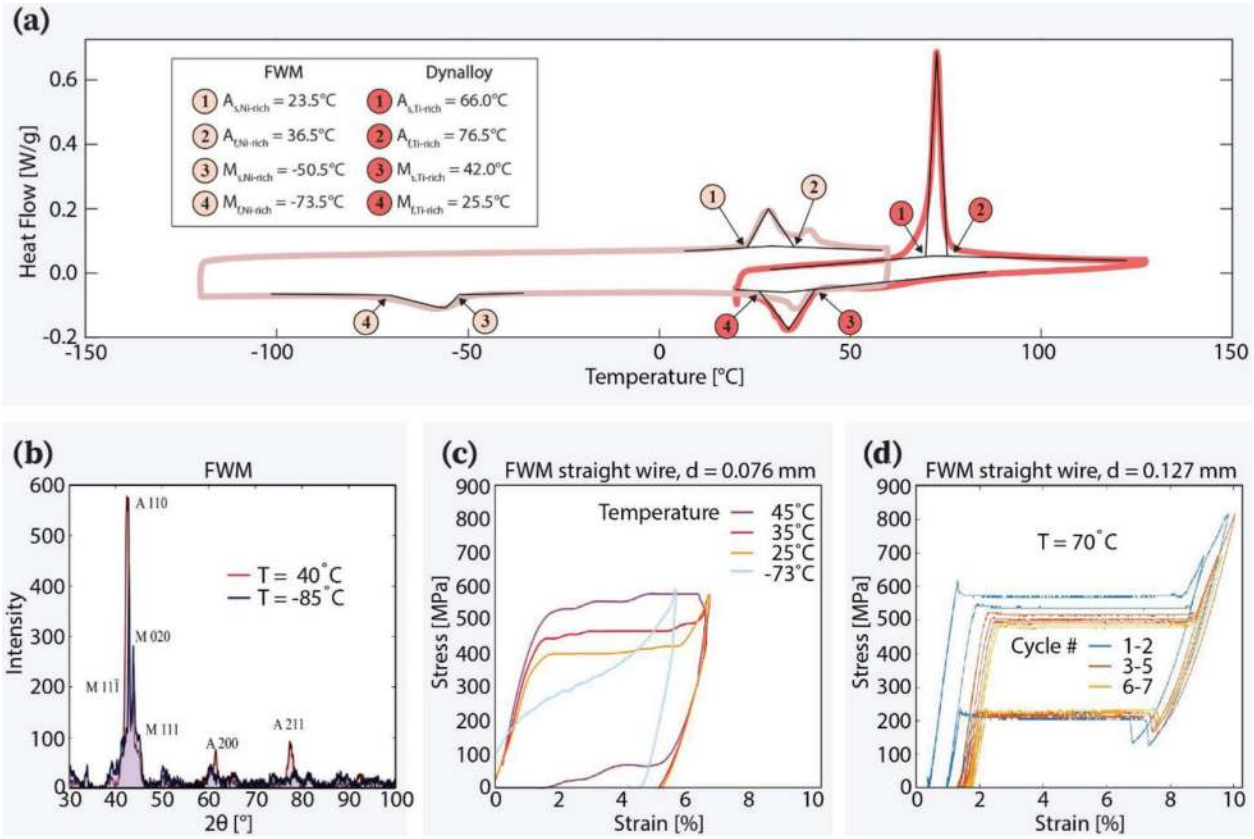

Figure 5.

a) DSC curves to compare 90 °C Flexinol manufactured by Dynalloy and the custom material designed by Fort Wayne Metals to actuate on the surface of human skin. b) Microstructure characterization of custom Fort Wayne Metals material through X-ray diffraction shows the thermally-induced austenite and martensite material states. c) Stress–strain data for custom Fort Wayne Metals material at varying temperatures (T = [45, 34, 25, and −73 °C], $\dot{\varepsilon}$ = 4 × 10 $^{-4}$ 1/s, d = 0.076 mm) shows the characteristic NiTi temperature-dependent plateau. d) Cyclic stress–strain data for one sample (T = 70 °C, $\dot{\varepsilon}$ = 8 × 10 $^{-5}$ 1/s, d = 0.127 mm) shows material performance degradation and stabilization after 7 loading and unloading cycles.

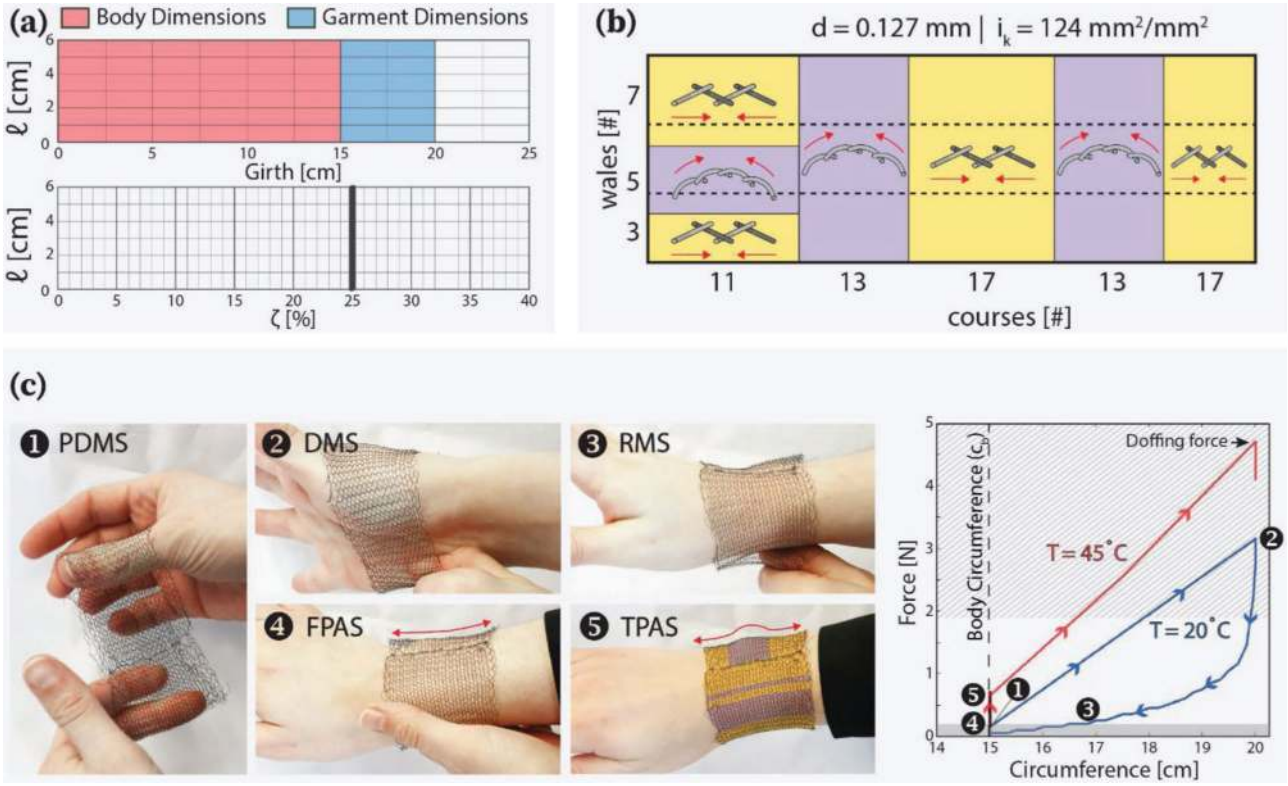

Figure 6.

a) Garment actuation contraction requirements (ζ_{req} = 25%) were defined by comparing the body dimension (i.e., wrist circumference) to the required garment dimensions to enable don/don (i.e., hand circumference). b) A wrist sleeve was designed using a SMA knitted actuator architecture that contracts up to 36% under low load (i.e., F = 50 g). Multiple knitted architectures (i.e., garter knit and knit-only) were incorporated into the design to improve fit around the curves of the wrist bone. c) A topographically conforming wrist sleeve prototype was designed with a small batch of custom NiTi fabricated by Fort Wayne Metals to implement unpowered, self-fitting with body heat. The sleeve performance was validated through thermomechanical testing to observe force-displacement behavior and evaluate implementation of the designed garment operation. 1) Pre-donned martensite state (PDMS): The martensitic wrist sleeve begins in room temperature under no load (T = 20 °C, F = 0 N). 2) Donned martensite state (DMS): The martensitic wrist sleeve is pulled over the largest part of the hand (T = 20 °C, F = 3.2 N). 3) Relaxed martensite state (RMS): Martensite relaxation causes the sleeve to contract slightly around the body; however, the sleeve remains oversized (T = 20 °C, F = 0 N). 4) Fitted, partially austenite state (FPAS): The palm is used to assist the material in warming to skin temperature (T = 45 °C, F > 0 N). 5) Tight, partially austenite state (TPAS): The warmed sleeve self-fits around the curvature of the wrist (T = 45 °C, F = 0.7 N), exerting low forces under 10 mmHg (F_{crit} = 1.9 N). To doff the garment, the warmed, fitted sleeve is manually pulled off the body with low forces (T = 45 °C, F = 4.7 N). The grey box (F = 0–0.2 N) represents the area of the 25 lb load cell that cannot be resolved.